

## Original Research

# A nomogram model integrating LI-RADS features and radiomics based on contrast-enhanced magnetic resonance imaging for predicting microvascular invasion in hepatocellular carcinoma falling the Milan criteria

Hai-Feng Liu<sup>a</sup>, Yan-Zhen-Zi Zhang<sup>b</sup>, Qing Wang<sup>a</sup>, Zu-Hui Zhu<sup>a</sup>, Wei Xing<sup>a,\*</sup>

<sup>a</sup> Department of Radiology, Third Affiliated Hospital of Soochow University, Changzhou 213000, Jiangsu, China

<sup>b</sup> Department of Pathology, Third Affiliated Hospital of Soochow University, Changzhou 213000, Jiangsu, China

## ARTICLE INFO

## Keywords:

Nomogram  
Radiomics  
Microvascular invasion (MVI)  
Hepatocellular carcinoma (HCC)  
Milan criteria

## ABSTRACT

**Purpose:** To establish and validate a nomogram model incorporating both liver imaging reporting and data system (LI-RADS) features and contrast enhanced magnetic resonance imaging (CEMRI)-based radiomics for predicting microvascular invasion (MVI) in hepatocellular carcinoma (HCC) falling the Milan criteria.

**Methods:** In total, 161 patients with 165 HCCs diagnosed with MVI ( $n = 99$ ) or without MVI ( $n = 66$ ) were assigned to a training and a test group. MRI LI-RADS characteristics and radiomics features selected by the LASSO algorithm were used to establish the MRI and Rad-score models, respectively, and the independent features were integrated to develop the nomogram model. The predictive ability of the nomogram was evaluated with receiver operating characteristic (ROC) curves.

**Results:** The risk factors associated with MVI ( $P < 0.05$ ) were related to larger tumor size, nonsmooth margin, mosaic architecture, corona enhancement and higher Rad-score. The areas under the ROC curve (AUCs) of the MRI feature model for predicting MVI were 0.85 (95% CI: 0.78–0.92) and 0.85 (95% CI: 0.74–0.95), and those for the Rad-score were 0.82 (95% CI: 0.73–0.90) and 0.80 (95% CI: 0.67–0.93) in the training and test groups, respectively. The nomogram presented improved AUC values of 0.87 (95% CI: 0.81–0.94) in the training group and 0.89 (95% CI: 0.81–0.98) in the test group ( $P < 0.05$ ) for predicting MVI. The calibration curve and decision curve analysis demonstrated that the nomogram model had high goodness-of-fit and clinical benefits.

**Conclusions:** The nomogram model can effectively predict MVI in patients with HCC falling within the Milan criteria and serves as a valuable imaging biomarker for facilitating individualized decision-making.

## Introduction

Hepatocellular carcinoma (HCC) is the most common type of primary liver cancer with the fifth highest incidence and has the third highest mortality rate globally due to its late-stage diagnosis and poor prognosis [1,2]. Currently, the Milan criteria (one HCC  $\leq 5$  cm or three HCCs  $\leq 3$  cm without extrahepatic metastasis or major vessel invasion), which align with early-stage HCC, are discriminatory in regard to selecting patients with clinical benefits for surgical resection or transplantation [3], while inhibitor-based immunotherapy or metronomic capecitabine are first-line therapies for advanced-stage HCC [4]. Microvascular invasion (MVI) is widely recognized as a crucial risk factor associated with early recurrence and poor prognosis in HCC

patients after therapy because of its aggressive biological behavior [5]; thus, the potential presence of MVI is recommended with a wide resection margin, inappropriate inclusion criteria for liver transplantation and frequent disease monitoring in HCC patients [6,7]. Therefore, preoperative prediction of MVI in HCC patients meeting the Milan criteria has particular clinical significance for guiding early-stage treatment decisions and improving patient outcomes.

Recent studies have shown the possibility of predicting MVI with serological tests, and the clinical utility of serum markers such as alpha-fetoprotein and total bilirubin in predicting MVI is inevitably limited by their relatively low diagnostic accuracy [8–11]. Fortunately, MRI features were indicated to be more valuable for predicting MVI, but these qualitative findings have been inconsistent, and interobserver

\* Corresponding author at: No.185, Juqian ST, Tianning District, Changzhou 213003, Jiangsu, China.

E-mail address: [suzhxingwei@suda.edu.cn](mailto:suzhxingwei@suda.edu.cn) (W. Xing).

variability was evident in a growing number of studies [10]. This is partly because few studies have applied the liver imaging reporting and data system (LI-RADS) to predict MVI in HCC following the Milan criteria, which provides a comprehensive and standardized interpretation of HCC imaging with major and ancillary features [12]. Moreover, radiomics can be used for evaluating regional microscopy of tumors at the millimeter scale by extracting quantitative signatures and has demonstrated promising performance for the prediction of MVI [13,14]. However, radiomics based on contrast-enhanced MRI (CEMRI) for the prediction of MVI in patients with HCC falling into the Milan criteria has not been explored until now. Thus, the development of a combined model incorporating LI-RADS features and radiomics derived from CEMRI to predict MVI in HCC patients falling into the Milan criteria is desirable.

The nomogram is one of the most effective prediction models, as it is evidence-based and individualized, enabling preoperative diagnosis and facilitating clinical decision-making of tumors with high accuracy and ease of understanding [15,16]. To provide a noninvasive imaging biomarker for the preoperative prediction of MVI, this study aimed to identify and validate a unique nomogram model that integrates LI-RADS characteristics and radiomics based on CEMRI to predict MVI in HCC patients meeting the Milan criteria.

## Materials and methods

### Patients

This retrospective study was approved by the Institutional Ethics Committee (2022-CL027-01), and the requirement for informed consent was waived. From June 2016 to June 2022, a total of 265 consecutive patients with HCC confirmed by pathology were analyzed. Patients meeting the following criteria were excluded: 1) preoperative CEMRI examination of the upper abdomen was absent; 2) HCC diagnosis did not satisfy the Milan criteria (one HCC  $\leq$  5 cm or three HCCs  $\leq$  3 cm without macrovascular invasion or extrahepatic metastasis) according to CEMRI findings; 3) interval time between CEMRI and pathology was more than one month; 4) HCC-related therapy prior to surgical resection; 5) poor CEMRI image quality owing to breathing artifacts; and 6) incomplete pathological descriptions of MVI.

Ultimately, 161 patients were enrolled and then randomly assigned

to the training group ( $n = 112$ ) or the test group ( $n = 49$ ) at a ratio of 7:3 according to the CEMRI number order. The process of patient selection is shown in Fig. 1.

### MVI analysis

MVI analysis was performed by one well-trained pathologist (15 years of experience in liver pathology) who was unaware of the preoperative data. MVI was defined as the microscopic presence of tumor cell nests in the portal vein, hepatic vein or large capsular vessel lined by endothelial cells and was classified into three pathological grades: a) M0: no MVI; b) M1: less than 5 MVI occurring in a peritumor ( $<1$  cm); M2: more than 5 MVI found in distant liver tissues ( $>1$  cm).

### MRI protocol and LI-RADS interpretation

MRI was performed in a 3.0-T Magnetom scanner (Verio, Siemens Healthiners, Germany) with a 12-channel abdominal matrix coil, with the following protocol: 1) in-phase and out-phase T1-weighted imaging (T1WI) in turbo-spin-echo; 2) fast spin-echo T2-weighted imaging (T2WI); 3) T2WI with fat-suppressed fast spin-echo; and 4) diffusion weighted imaging (DWI) in echo planar imaging with a b value = 0, 800 s/mm [2]. 5) For gadoteric acid contrast enhancement, images for the precontrast phase of T1WI, arterial phase (AP, 25~35 s), portal venous phase (PVP, 60~70 s) and delayed phase (DP, 180 s) were obtained with 3D volumetric interpolated breath-hold examination (VIBE) techniques after injecting 0.2 ml/kg Gd (Gd-DTPA, Magnevist, Bayer Schering Pharma, Berlin, Germany) at a bolus rate of 1 ml/s prior to a 20 ml saline flush using a power injector. Finally, 10~15 min were required for a complete MRI examination. The detailed sequence and parameters are shown in Table S1.

Two radiologists with 7 years (HFL) and 12 years (QW) of experience in liver MR imaging who were blinded to the pathology results analyzed the MRI images, and any discrepancies were settled by consensus. The following LI-RADS (v2018) features were analyzed [12]: (a) major features: nonrim arterial phase hyperenhancement (NAPHE), non-peripheral washout, and enhancing capsule; (b) ancillary features favoring HCC in particular: nonenhancing capsule, nodule-in-nodule, mosaic architecture, blood products in the tumor, and higher fat content in the mass than in the adjacent liver tissue; (c) ancillary features

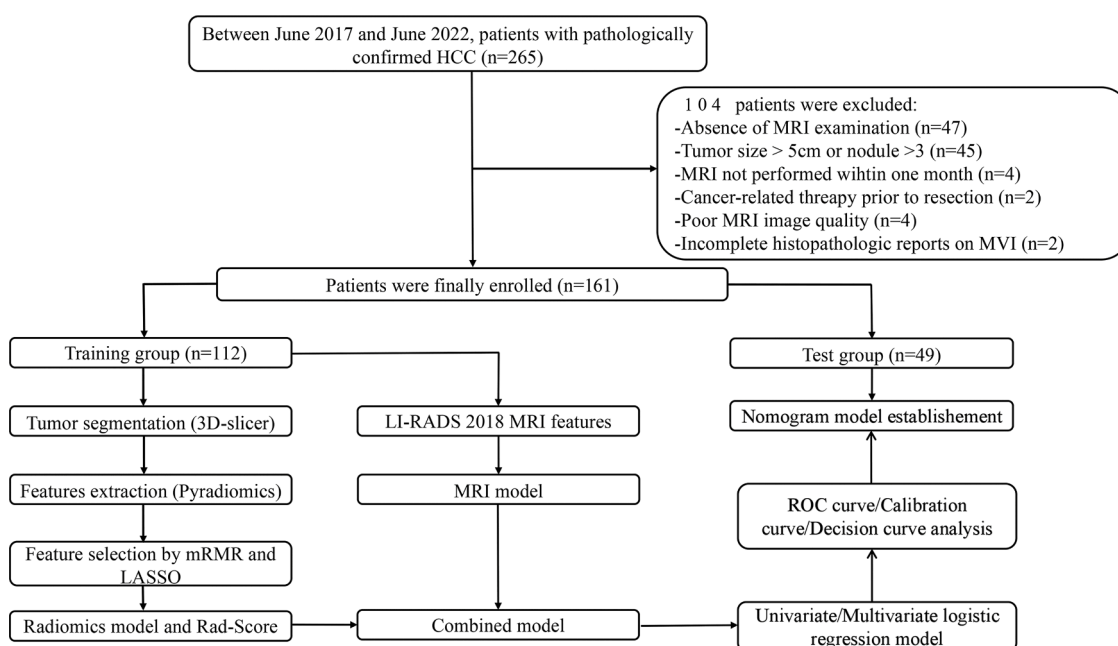


Fig. 1. The detailed flowchart from patient selection to nomogram model establishment is shown in Fig. 1.

favoring malignancy but not HCC in particular: restricted diffusion, mild-moderate T2 hyperintensity, corona enhancement, fat sparing in the tumor, and iron sparing in the tumor; (d) baseline findings of HCCs: tumor size, margin (nonsmooth or smooth), shape (irregular or regular).

#### Tumor segmentation and extraction of radiomics features

3D-Slicer software (version 5.0.3; <http://www.slicer.org>) was used to extract radiomics features from the AP, PVP and DP images by a radiologist (HFL). First, all images were resampled with linear interpolation algorithms at a voxel spacing of  $1 \times 1 \times 1$  mm to correct the pixel-spacing differences and reduce the heterogeneity. Afterward, the 3D region of interest (ROI) that covered the entire tumor volume was manually delineated along the tumor boundary on each consecutive transverse slice. Notably, the ROI needed to include the area of necrosis and hemorrhage within the HCC and to exclude visible satellite lesions.

The Pyradiomics package (Version 2.1.2, <http://www.radiomics.io/pyradiomics.html>) was used to extract 107 radiomics features from each CEMRI sequence. The radiomics features consisted of the following: I) shape features ( $n = 14$ ), 3D shape-related features; II) first-order histogram features ( $n = 18$ ), spatial distribution of multiple voxel values; III) texture features ( $n = 75$ ), heterogeneity differences via a density histogram and the relative spatial locations of pixels, including 24 gray-level cooccurrence matrix (GLCM) features, 14 gray-level dependence matrix (GLDM) features, 16 gray-level run-length matrix (GLRLM) features, 16 gray-level size zone matrix (GLSZM) features, and 5 neighboring gray-tone difference matrix (NGTDM) features. Overall, a total of 321 features were extracted for every HCC.

#### Feature selection and radiomics model development

Three-step procedures were conducted sequentially to reduce dimensionality and identify the optimal radiomics for predicting MVI. Before feature selection, all extracted radiomics features were standardized by the Z score method. First, MRI images of forty patients were randomly selected for resegmentation and feature extraction twice by the same radiologist (HFL) and another senior radiologist (QW). Then, both intra- and interradiologist intraclass correlation coefficients (ICCs)  $> 0.70$  for those 40 cases served as the inclusion criteria to select stable features for further analysis. Second, the maximum relevance minimum redundancy (mRMR) method was adopted to reduce dimensionality and to eliminate redundant and irrelevant features. Third, the least absolute shrinkage and selection operator (LASSO) algorithm was applied to identify the most valuable features with nonzero coefficients after the 10-fold cross-validation penalty procedure for predicting MVI. Finally, the radiomics score (Rad-score) was calculated and constructed for each HCC lesion through a linear combination of selected features that were weighted by their respective coefficients.

#### Nomogram model establishment and verification

To predict the probability of MVI in HCC falling within the Milan criteria, a nomogram was generated by integrating LI-RADS features and the Rad-score. Univariate and multivariate logistic regression analyses were conducted to identify risk factors associated with MVI, and these independent factors were incorporated to establish a predictive nomogram model in the training groups by regression analysis and were verified in the test groups. Then, a calibration curve with the Hosmer–Lemeshow test and decision curve analysis (DCA) were used to evaluate the goodness-of-fit and net clinical benefits of the nomogram model in predicting MVI, respectively.

#### Statistical analysis

Statistical analyses were performed using the R software-integrated EmpowerStats software [17] (version 4.0; <http://www.empowerstats.com/cn/>).

Continuous variables were described as the mean  $\pm$  standard deviation or median (interquartile range) after a normality distribution test with the Shapiro–Wilk method, and categorical variables were shown as percentages. Independent t tests (normal distribution) or Mann–Whitney U tests (skewed distribution) and chi-square ( $\chi^2$ ) or Fisher's tests were performed to detect significant differences between the MVI (+) and MVI (-) groups. The diagnostic efficiency of the three models (MRI features, Rad-score, and nomogram) in discriminating MVI was evaluated with receiver operating characteristic (ROC) curves. Sensitivity, specificity, accuracy, and the area under the ROC (AUC) were calculated, and the difference in AUC value among different models was compared by the Delong method. For all tests, a two-tailed  $P$  value of  $< 0.05$  was considered statistically significant. The detailed flowchart from patient selection to nomogram model establishment is shown in Fig. 1.

## Results

#### Baseline characteristics of participating patients

In this study, a total of 161 patients (male/female: 123/38; mean age:  $62.9 \pm 10.1$  years) were included and randomly divided into training ( $n = 112$ ) and test ( $n = 49$ ) groups. Notably, four patients (3 in the training group and 1 in the test group) presented two HCCs. Among the 165 HCCs, 40.0% (66/165) were pathologically identified as having MVI (MVI+), and 60.0% (99/165) were confirmed to have no MVI (MVI-). Furthermore, 40.0% (46/115) and 40.0% (20/50) of HCCs were confirmed as MVI+ in the training and test groups, respectively. No significant differences were found in age, sex, etiology, cirrhosis, HCC number, MVI presence, alpha-fetoprotein (AFP), alanine aminotransferase (ALT), aspartate aminotransferase (AST), or total bilirubin (TB) between the training and test groups. The baseline characteristics of the participating patients are shown in Table 1.

#### Diagnostic performance of the MRI feature model

Regarding various LI-RADS MRI features, larger tumor size ( $>3$  cm), nonsmooth margins, nodule-in-nodule, mosaic architecture and corona enhancement were indicated to be independent factors associated with MVI ( $P < 0.05$ ), with no other significant differences found between the two groups ( $P > 0.05$ ), as shown in Table 2. The typical MRI features for MVI+ in HCC patients are shown in Fig. 2. After combining these significant MRI features, the MRI feature model for predicting MVI in HCC falling within the Milan criteria presented a sensitivity of 89.13%, a specificity of 66.67% and an AUC value of 0.85 (95% CI: 0.78–0.92) in the training group, and they were 80.00%, 73.33% and 0.85 (95% CI: 0.74–0.95) for the test group, respectively.

#### Rad-score model construction

Fig. 3 shows the detailed workflow of feature selection and Rad-score model construction. After excluding radiomics signatures with  $ICC < 0.70$ , 97, 99, and 97 stable features remained for AP, PVP and DP, respectively. Through mRMR, thirty features (14 with AP, 9 with PVP, and 7 with DVP) were retained for LASSO. Ultimately, the six most valuable features associated with MVI were combined to construct the Rad-score model based on the following formula: Rad-score =  $0.30464 \times \text{Shape-MajorAxisLength}_{AP} + 0.04237 \times \text{Glcm-Correlation}_{AP} - 0.02774 \times \text{Glrlm-RunVariance}_{AP} - 0.04997 \times \text{Glszm-ZoneVariance}_{AP} + 0.13854 \times \text{Glszm-SmallAreaLowGrayLevelEmphasis}_{PVP} + 0.19174 \times \text{First-order-Skewness}_{DP}$ . The sensitivity, specificity and AUC value of the Rad-score model in predicting MVI were 80.43%, 73.91% and 0.82 (95% CI: 0.73–0.90) for the training group and 60.00%, 96.67% and 0.80 (95% CI: 0.67–0.93) for the test group, respectively.

**Table 1**  
Baseline characteristic of enrolled patients.

	Total (n = 161)	Training group (n = 112)	Test group (n = 49)	t/χ <sup>2</sup> /Z	P value
Age (Years)	62.9 ± 10.1	62.9 ± 9.6	62.9 ± 11.4	0.03	0.98
Gender					
Male	123 (76.4%)	85(75.9%)	38(77.6%)	0.23	0.41
Female	38(23.6%)	27(24.1%)	11(22.4%)		
Etiology					
HBV/HCV	124 (77.0%)	86(76.8%)	38(77.6%)	0.11	0.46
Other-None	37(23.0%)	26(23.2%)	11(22.4%)		
AFP					
≥20 ng/ml	67(41.6%)	46(41.1%)	14(28.6%)	0.21	0.42
<20 ng/ml	94(58.4%)	66(58.9%)	28(71.4%)		
ALT (U/L)	72.0 ± 108.6	75.1 ± 115.9	64.9 ± 90.4	-0.60	0.55
AST(U/L)	73.7 ± 156.7	82.6 ± 183.5	53.4 ± 58.2	-1.52	0.13
TB (μmol/L)	17.5 ± 28.5	16.1 ± 8.1	20.6 ± 31.2	0.99	0.32
Cirrhosis					
Present	71(44.1%)	61(54.5%)	20(40.8%)	-0.56	0.29
Absent	90(55.9%)	51(45.5%)	29(59.2%)		
No. of HCC					
Solitary	157 (97.5%)	109(97.3%)	48(98.0%)	1.34	0.51
Two	4(2.5%)	3(2.7%)	1(2.0%)		
MVI presence					
M0	99(60.0%)	69(60.0%)	30(60.0%)	5.60	0.06
M1	46(27.9%)	28(24.3%)	18(36.0%)		
M2	20(12.1%)	18(15.7%)	2(4.0%)		

HBV, hepatitis B virus; HCV, hepatitis C virus; AFP, alpha-fetoprotein; ALT, alanine aminotransferase; AST, aspartate aminotransferase; No, number; MVI, microvascular invasion.

Note: MVI incidence was calculated based on the number of HCC (n = 165).

#### Univariate and multivariate analyses of risk factors associated with MVI

Univariate analysis demonstrated that significant risk factors for MVI were related to larger size (OR=6.9, 95% CI: 3.0–16.1,  $P < 0.001$ ), nonsmooth margins (OR=3.0, 95% CI: 1.2–7.6,  $P = 0.02$ ), nodule-in-nodule (OR=10.2, 95% CI: 1.2–87.8,  $P = 0.03$ ), mosaic architecture (OR=4.1, 95% CI: 1.9–9.1,  $P < 0.001$ ), corona enhancement (OR=8.4, 95% CI: 3.6–19.7,  $P < 0.001$ ) and higher Rad-score (OR=108.1, 95% CI: 17.2–680.7,  $P < 0.001$ ).

After multivariate analysis, the retained independent predictors for MVI in HCC falling Milan criteria were related to larger size (OR=4.1, 95% CI: 1.3–12.9,  $P = 0.02$ ), nonsmooth margin (OR=4.4, 95% CI: 1.1–18.0,  $P = 0.04$ ), mosaic architecture (OR=3.2, 95% CI: 1.0–9.6,  $P = 0.04$ ), corona enhancement (OR=3.7, 95% CI: 1.1–12.2,  $P = 0.03$ ) and higher Rad-score (OR=10.2, 95% CI: 1.0–102.2,  $P = 0.04$ ), as presented in Table 3.

#### Nomogram model establishment and validation

The established nomogram model (Fig. 4) derived from the above five independent predictors demonstrated AUC values of 0.87 (95% CI: 0.81–0.94) and 0.89 (95% CI: 0.81–0.98) for predicting MVI in HCC falling into the Milan criteria in the training and test groups (Fig. 5A–5B), respectively, as shown in Table 4. The calibration curves suggested that the predictive nomogram and the actual probability of MVI were well fitted in both the training (Fig. 5C) and test (Fig. 5D) groups. Additionally, the DCA results showed that the predictive nomogram curve was higher than the default lines for either all or none of the patients having MVI over all reasonable threshold probabilities (Fig. 5E–F).

Furthermore, the combined nomogram model demonstrated better

performance than the MRI features and the Rad-score model for predicting MVI in HCC falling into the Milan criteria, with AUC values of 0.87 vs. 0.85 ( $P = 0.13$ ) for the nomogram compared with the MRI features and 0.87 vs. 0.82 ( $P = 0.02$ ) for the nomogram compared with the Rad-score model. However, no significant difference in the AUC value (0.85 vs. 0.82,  $P = 0.30$ ) was found in the comparison between the MRI features and the Rad-score model, as shown in Fig. 5 and Table 4.

#### Discussion

In this study, we established and verified a nomogram model integrating qualitative LI-RADS features and quantitative radiomics signatures derived from CEMRI for the prediction of MVI in HCC falling within the Milan criteria. We concluded that a larger tumor size (HCC > 3 cm), nonsmooth margins, mosaic architecture, corona enhancement and higher Rad-score were significantly associated with MVI, and both MRI features and the Rad-score model were important in predicting MVI. Moreover, the combined nomogram model exhibited improved diagnostic ability with high goodness-of-fit and improved clinical benefits in predicting MVI compared with the MRI features model or the Rad-score model alone, indicating the effectiveness of this combined imaging tool in preoperatively predicting MVI and in assisting individualized decision-making in HCC patients who fall within the Milan criteria.

A recent meta-analysis demonstrated that an HCC tumor diameter > 5 cm was significantly associated with MVI and showed a pooled specificity of 89.3% (95% CI: 81.4–94.1) for predicting MVI [10], as also reported by Rungsakulkij N [18]. However, a few studies have been conducted to predict MVI using a 3 cm HCC tumor diameter as the diagnostic value, and the 5-year overall survival and recurrence-free survival rates of patients in the HCC ≤ 3 cm group were 67.8% and 52%, respectively, significantly higher than the corresponding survival rates of 42.3% and 29.3% in the HCC > 3 cm group [19]. In this study, HCC size > 3 cm was identified as an independent predictor of MVI, because larger tumors are more likely to exhibit infiltrative growth and to destroy the peritumoral capsule [20]. This suggests that a 3 cm diameter is a crucial threshold in preoperatively predicting MVI for HCC falling within the Milan criteria, which is useful insight for improving the current understanding regarding HCC size criteria for surgical resection or liver transplantation. Nonsmooth margins are described as being of multicentric origin and of the multinodular type or as invasive growth in solitary nodules that are densely vascularized, indicating the malignant biological behavior of tumor capsule destruction and protrusion into the nontumoral parenchyma [21]; thus, nonsmooth margins are associated with MVI risk in HCC. The nodule-in-nodule feature was a risk factor associated with MVI in the training group, which was in accordance with Wei et al. [22] but presented an insignificant difference in the test group and was excluded from multivariate analysis, indicating that the nodule-in-nodule feature was unstable in predicting MVI in HCC within Milan criteria.

The mosaic architecture is characteristically composed of random compartments or internal nodules that differ in enhancement, attenuation, intensity, shape, size and separation by fibrous tissues within a tumor. Pathologically, this architecture reflects tumor viability, fatty infiltration, hemorrhage, necrosis or copper deposition [23]. Therefore, the observation that the mosaic architecture is accompanied by rapid disease progression, diverse biological heterogeneities and a greater propensity for vascular invasion contributed to the results in this study; the mosaic architecture was more frequently observed and was a risk factor associated with MVI. However, mosaic architecture features were not considered a risk factor for MVI in the study of Wei et al. [22], who speculated that their study included a relatively large number of HCCs > 5 cm (45.9%), which demonstrated a higher rate of mosaic architecture features. Corona enhancement indicates drainage of the contrast agent from the HCC tumor into the peritumoral parenchyma and appears as peritumoral enhancement during PVP or DP, reflecting vascular

**Table 2**  
LI-RADS MRI features and Rad-Score of included patients in the training and test groups.

MRI characteristics	Training group			Test group			$P_{inter}$
	MVI + (n = 46)	MVI - (n = 69)	$P_{intra}$	MVI + (n = 20)	MVI - (n = 30)	$P_{intra}$	
Tumor size (>3/≤3 cm)	34(73.9%)/12 (26.1%)	20(29.0%)/49 (71.0%)	<0.001*	13(65.0%)/7 (35.0%)	17(56.7%)/13 (43.3%)	0.007*	0.13
Tumor margin (Nonsmooth/Smooth)	39(84.8%)/7 (15.2%)	45(65.2%)/24 (34.8%)	0.02*	16(80.0%)/4 (20.0%)	12(40.0%)/18 (60.0%)	0.005	0.03*
Tumor shape (Irregular/ Regular)	31(67.4%)/15 (32.6%)	56(81.2%)/13 (18.8%)	0.09	15(75.0%)/5 (25.0%)	17(56.7%)/13 (43.3%)	0.19	0.14
<b>Major features</b>							
NAPHE (Present/ Absent)	41(89.1%)/5 (10.9%)	61(88.4%)/8 (11.6%)	0.90	20(100.0%)/0 (0.0%)	27(90.0%)/3 (10.0%)	0.15	0.40
Nonperipheral washout (Present/ Absent)	43(93.5%)/3 (6.5%)	60(87.0%)/9 (13.0%)	0.26	19(95.0%)/1 (5.0%)	25(83.3%)/5 (16.7%)	0.21	0.59
Enhancing capsule (Present/ Absent)	42(91.3%)/4 (8.7%)	63(91.3%)/6 (8.7%)	1.00	19(95.0%)/1 (5.0%)	27(90.0%)/3 (10.0%)	0.52	0.88
<b>Ancillary features, favoring HCC in particular</b>							
Nonenhancing capsule (Present/ Absent)	0(0.0%)/66 (100.0%)	0(0.0%)/69 (100.0%)	1.00	0(0.0%)/20 (100.0%)	0(0.0%)/30 (100.0%)	1	1
Nodule-in-nodule (Present/ Absent)	6(13.0%)/40 (87.0%)	1(1.4%)/68 (98.6%)	0.01*	2(10.0%)/18 (90.0%)	1(3.3%)/29 (96.7%)	0.33	0.02*
Mosaic architecture (Present/ Absent)	31(67.4%)/15 (32.6%)	23(33.3%)/46 (66.7%)	<0.001*	14(70.0%)/6 (30.0%)	10(33.3%)/20 (66.7%)	0.01	0.90
Blood products (Present/ Absent)	9(19.6%)/37 (80.4%)	8(11.6%)/61 (88.4%)	0.24	1(5.0%)/19 (95.0%)	3(10.0%)/27 (90.0%)	0.52	0.31
Fat in tumor (Present/ Absent)	4(8.7%)/42 (91.3%)	6(8.7%)/63 (91.3%)	1.00	1(5.0%)/19 (95.0%)	0(0.0%)/30 (100.0%)	0.22	0.18
<b>Ancillary features favoring malignancy, not HCC in particular</b>							
Restricted diffusion (Present/ Absent)	45(97.8%)/1 (2.2%)	66(95.7%)/3 (4.3%)	0.53	20(100.0%)/0 (0.0%)	29(96.7%)/1 (3.3%)	0.41	0.61
Mild-moderate T2 hyperintensity (Present/ Absent)	45(97.8%)/1 (2.2%)	66(95.7%)/3 (4.3%)	0.53	20(100.0%)/0 (0.0%)	28(93.3%)/2 (6.7%)	0.24	0.87
Corona enhancement (Present/ Absent)	33(71.7%)/13 (28.3%)	16(23.2%)/53 (76.8%)	<0.001*	13(65.0%)/7 (35.0%)	9(30.0%)/21 (70.0%)	0.02	<0.87
Fat sparing in tumor (Present/ Absent)	5(10.9%)/41 (89.1%)	2(2.9%)/67 (97.1%)	0.73	1(5.0%)/19 (95.0%)	1(3.3%)/29 (96.7%)	0.77	0.74
Iron sparing in tumor (Present/ Absent)	1(2.2%)/45 (97.8%)	0(0.0%)/69 (100.0%)	0.40	0(0.0%)/20 (100.0%)	0(0.0%)/30 (100.0%)	1.00	1.00
Rad-Score	0.18±0.27	-0.18±0.28	<0.001*	0.16±0.28	-0.14±0.18	<0.001*	<0.001*

LI-RADS, liver imaging reporting and data system; NAPHE, non-rim arterial phase hyperenhancement;  $P_{intra}$ , difference between the MVI+ and MVI- groups;  $P_{inter}$ , difference between the training and test groups. \*represents  $P < 0.05$ .

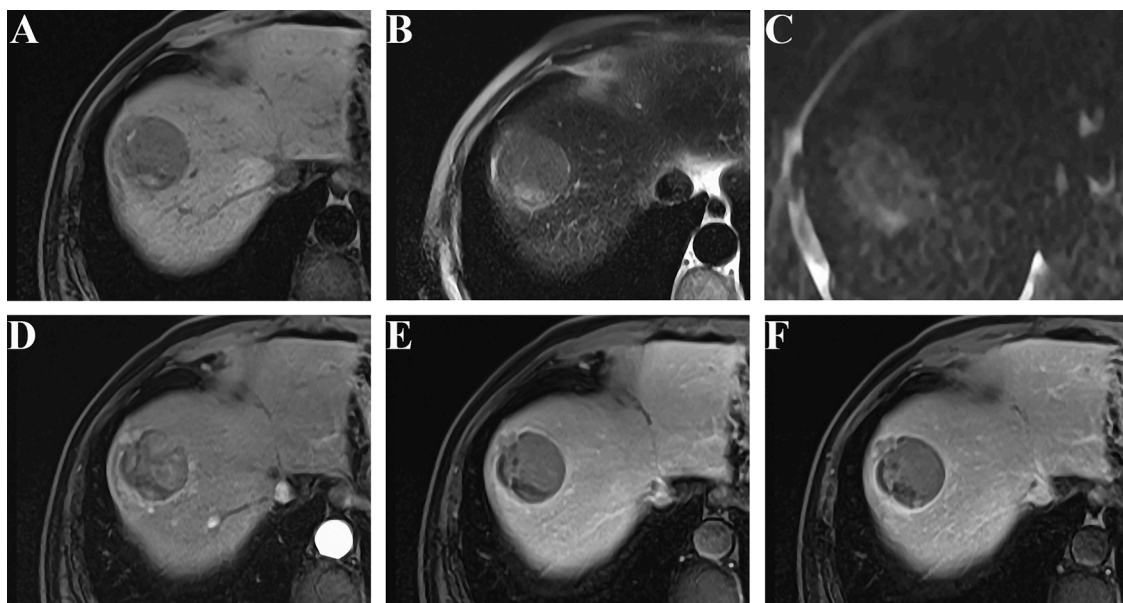


**Fig. 2.** Typical MRI features for MVI with HCC in a 58-year-old male patient. In the S8 lobe, a 4.3 × 4.0 cm sized irregular mass with nonsmooth margin showing T1 hypointensity with blood products (A), mild-moderate T2 hyperintensity (B), restricted diffusion (C), NAPHE feature (D) with subsequent washout and enhancing capsule on PVP and DP (E-F). Notably, mosaic architecture and corona enhancement were also present. After hepatectomy, M2 was pathologically diagnosed.

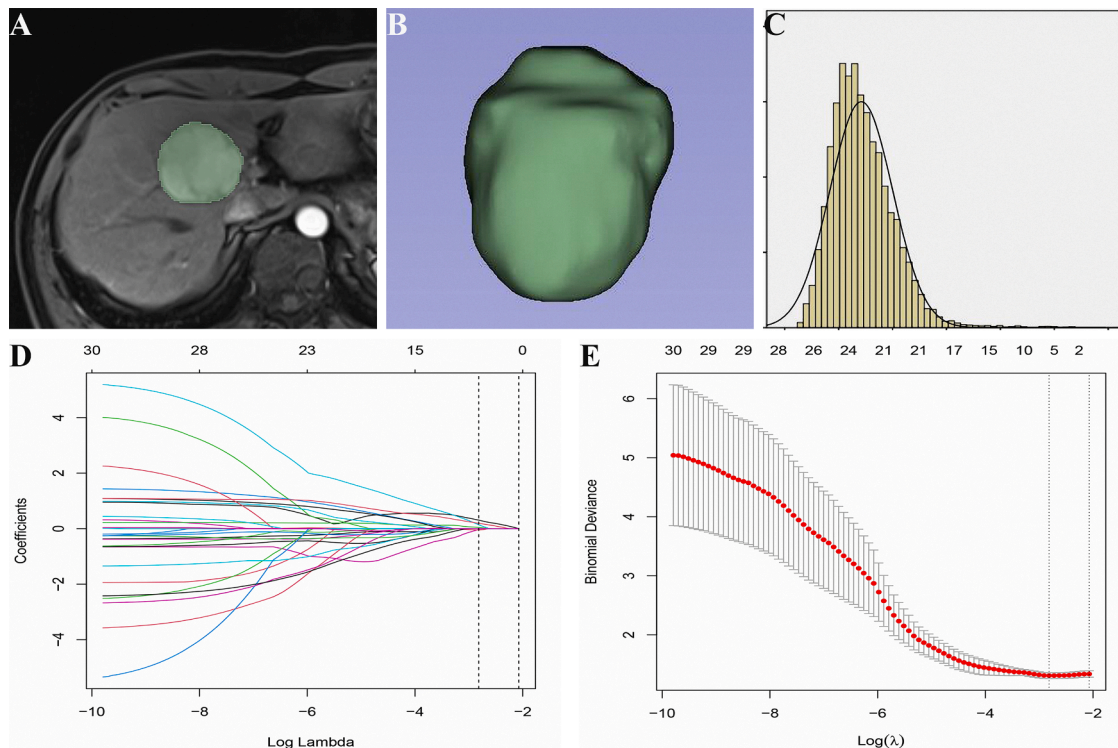


**Fig. 3.** The detailed workflow of radiomics model construction in a 64-year-old male with HCC. (A) Manual segmentation of the whole tumor in the AP; (B) 3D-shape, volumetric reconstruction of the ROI; (C) First-order histogram. Each colored line represents the corresponding coefficient of each feature, and LASSO adjusts  $\lambda$  (D). After tuning  $\lambda$  (E) in the LASSO model via tenfold cross-validation based on minimum criteria, the black vertical bar defines the best value of  $\lambda$ . The optimal weighting parameters  $\lambda = 0.0598$  and  $\text{Log}(\lambda) = -2.8162$  were selected, and six nonzero radiomics features were finally selected to construct the model.

**Table 3**  
Univariate and multivariate analysis for MVI with HCC in the training group.

Variables	Univariate Analysis			Multivariate Analysis		
	OR	95%CI	P value	OR	95%CI	P value
Tumor size (>3/≤3 cm)	6.9	3.0–16.1	<0.001*	4.1	1.3–12.9	0.02 *
Tumor margin (Nonsmooth/Smooth)	3.0	1.2–7.6	0.02*	4.4	1.1–18.0	0.04 *
Tumor shape (Irregular/ Regular)	1.1	0.4–3.1	0.81			
NAPHE (Present/ Absent)	1.1	0.3–3.5	0.90			
Nonperipheral washout (Present/ Absent)	2.1	0.5–8.4	0.27			
Enhancing capsule (Present/ Absent)	1.0	0.3–3.8	1.00			
Nodule-in-nodule (Present/ Absent)	10.2	1.2–87.8	0.03*	2.2	0.1–40.3	0.59
Mosaic architecture (Present/ Absent)	4.1	1.9–9.1	<0.001*	3.2	1.0–9.6	0.04*
Blood products (Present/ Absent)	1.9	0.7–5.2	0.24			
Fat in tumor (Present/ Absent)	1.0	0.3–3.8	1.00			
Restricted diffusion (Present/ Absent)	2.0	0.2–20.3	0.54			
Mild-moderate T2 hyperintensity (Present/ Absent)	2.0	0.2–20.3	0.54			
Corona enhancement (Present/ Absent)	8.4	3.6–19.7	<0.001*	3.7	1.1–12.2	0.03*
Fat sparing in tumor	1.1	0.2–5.3	0.87			
Iron sparing in tumor	0.0	0–∞	0.99			
Rad-score	108.1	17.2–680.7	<0.001*	10.2	1.0–102.2	0.04 *

invasion and intrahepatic metastases that can be visible as satellite nodules within the drainage vessels around HCC. This indicates that corona enhancement is an aggressive feature associated with HCC biological behavior [24]. Similarly, Zhang et al. [25] found that corona enhancement was associated with early recurrence in HCC patients meeting the Milan criteria after curative resection, emphasizing that corona enhancement is a key predictor of MVI and patient prognosis.

Moreover, the MRI feature model suggested good performance in predicting MVI, indicating its potential for interpreting the macroscopic and feature biological properties of HCC; however, the reproducibility and comparability limitations with the MRI features are major concerns

because of visual assessment. As a newly developed imaging technique, radiomics uses numerous microscopic signatures to quantitatively reflect tumor phenotypes, heterogeneities, microenvironments, and biological behaviors at the cellular and genetic levels [13,14]. In this study, six selected optimal radiomics features that were converted into quantitative Rad-scores were identified as independent predictors of MVI, suggesting that radiomics provided additional value to LI-RADS features for individualized MVI prediction. Considering the lack of highly accurate factors for predicting MVI, computational-assisted models integrating different prognostic and determinant factors associated with MVI have become a viable alternative for better clinical

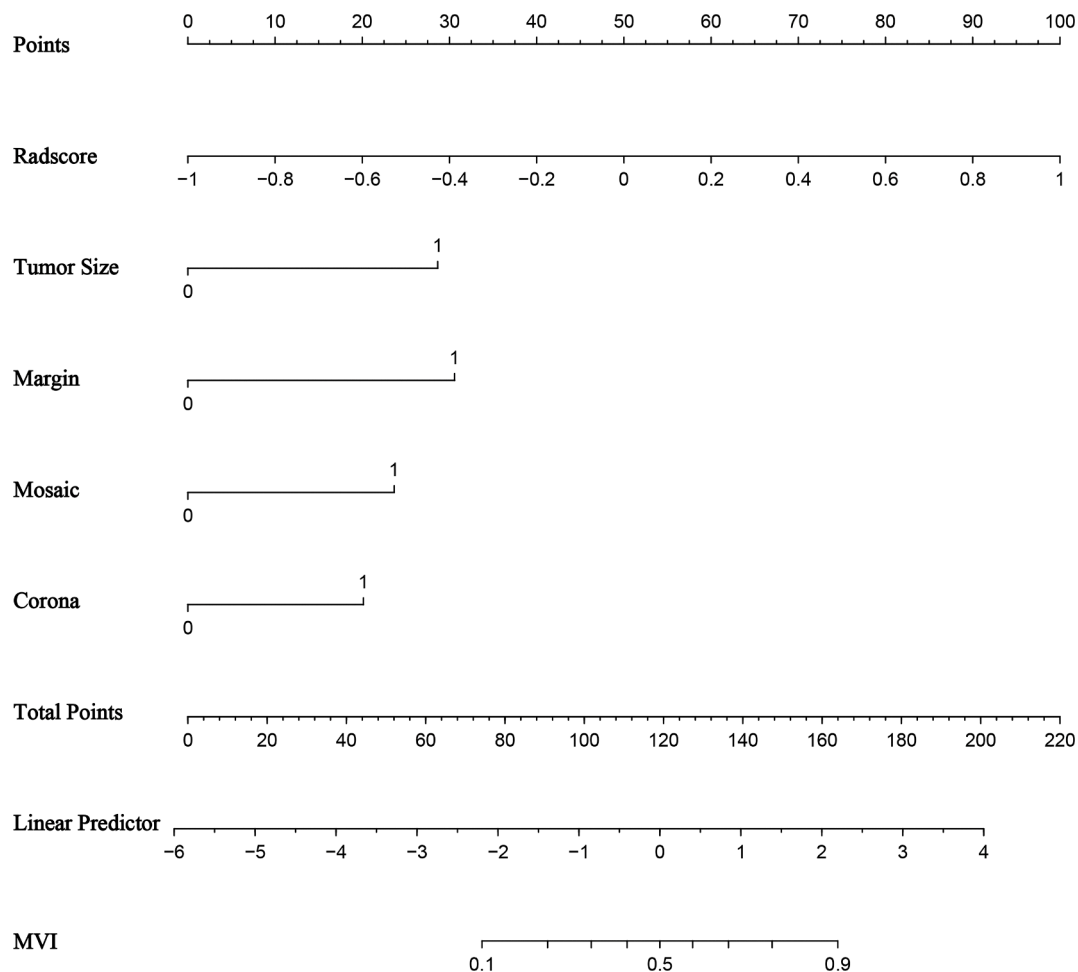


**Fig. 4.** The nomogram to predict MVI for HCC. To display the nomogram, first, all independent predictor points can be found on the line "Points". Then, the five predictor points are added to the line "Total Points". Finally, a vertical line is drawn downward from "Total Points" to the MVI status axes.

management. Lei et al. [26] established a nomogram by combining data related to tumor diameter, number, and capsule status as well as serum markers and MRI features to predict MVI in patients with hepatitis B (HBV)-related HCC within the Milan criteria, contributing to AUC values of 0.81 (0.78–0.85) and 0.80 (0.75–0.86) in the training and validation cohorts, respectively. Zhao et al. [27] developed a preoperative scoring model incorporating intratumoral arteries, nonnodular HCC type, and absence of a tumor capsule on contrast-enhanced computed tomography (CT) for predicting MVI with all reasonable tumor sizes, and this model had AUC values of 0.87 and 0.86 in the training and test groups, respectively.

In our study, this nomogram model incorporating LI-RADS and radiomics features based on CEMRI achieved satisfactory prediction of MVI with AUC values of 0.87 and 0.89 in the training and test groups, respectively. In addition, the calibration curve and DCA results demonstrated the high goodness-of-fit and clinical benefits of this nomogram. Notably, the nomogram model had a significantly higher AUC than the MRI features model and Rad-score models, indicating that it is an advisable and effective tool for predicting MVI and may provide references for subsequent treatments and clinical decision-making. Notably, among our risk factors, the Rad-score was more important than a single MRI feature in the nomogram model. This finding was in line with the results of Ji et al. [28], in which the radiomic signature was the top predictor, followed by clinicoradiologic factors, emphasizing the importance of radiomics in predicting MVI.

There are several limitations in this study. First, owing to the limited sample size and potential selection bias concerning the excluded

patients with absent preoperative CEMRI examination, which may negatively decrease the generalizability and reliability of our study results, multicenter prospective studies in larger cohorts are warranted to confirm the predictive ability of this nomogram model. Second, peritumoral hypointensity in the hepatobiliary phase (HBP) was identified as a risk factor associated with MVI [22], and it was hypothesized that tumor invasion of peritumor microvessels damages peritumoral hepatocytes and therefore reduces uptake of the contrast agent Gd-EOB-DTPA. However, the peritumoral manifestation on HBP was not discussed in this study because the contrast agent remains expensive and is not widely accessible to HCC patients. Third, to eliminate irrelevant signatures, the optimal radiomics features were merely extracted from CEMRI images, as CEMRI characteristics were the major features in diagnosing HCC, and the CEMRI image radiomics analysis findings were more similar to the actual tumor heterogeneity [29]; however, this selection procedure might exclude some potential features from DWI or T2WI [30]. Finally, this study only analyzed the relationship between MVI prediction and the nomogram model. We will increase the correlation between the nomogram model and recurrence and prognosis in future studies to make our research more clinically practical.

## Conclusion

In conclusion, larger tumor size, nonsmooth margins, mosaic architecture, corona enhancement and higher Rad-score were identified as effective imaging markers for preoperatively predicting MVI in patients with HCC falling into the Milan criteria. Moreover, the nomogram

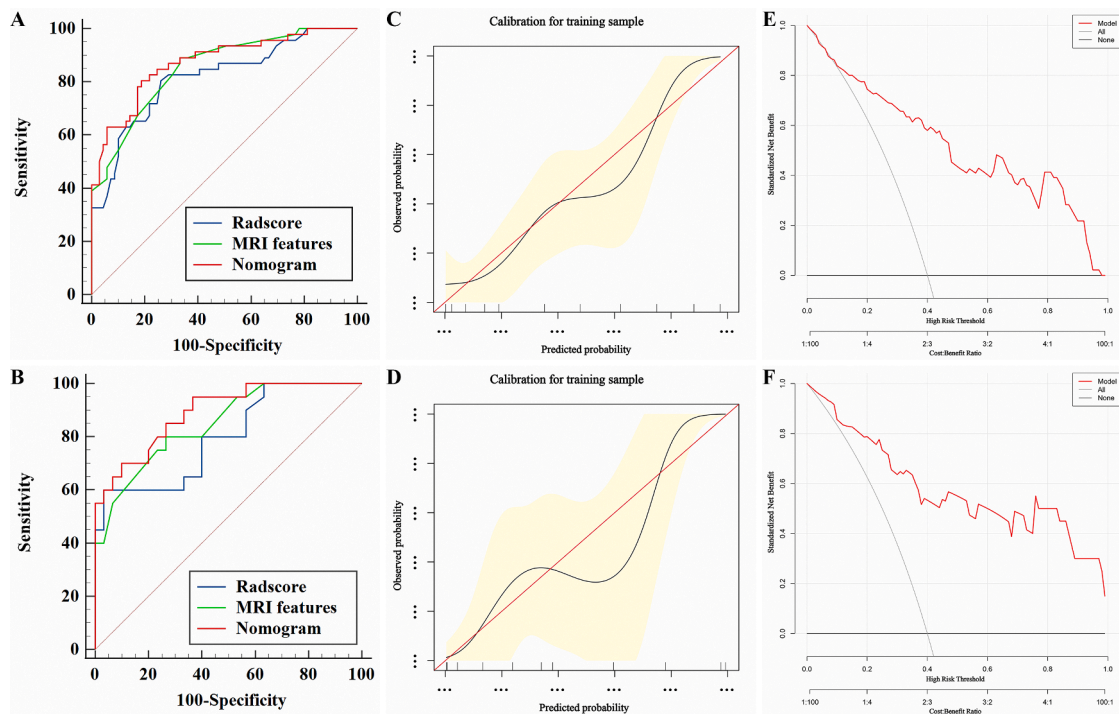


**Fig. 5.** The ROC curve (A-B), calibration curve (C-D), and DCA curve (E-F) of the nomogram model for predicting MVI in HCC within the Milan criteria in the training and test groups. Calibration curves depict the agreement of the nomogram model between the predicted risks (X-axis) of MVI and the actual observed MVI (Y-axis). The red solid line represents the performance of the nomogram, and the closer the red line is to the diagonal dashed line, the better the predictive efficacy of the nomogram. The nomogram model (red line) provides increased clinical benefit compared with both all (gray line) and none (horizontal black line) patients expressing MVI across a full range of reasonable threshold probabilities.

**Table 4**  
Diagnostic performance of the difference models in predicting MVI in HCC within Milan criteria.

Different models	Training group				P value	Test group			
	Accuracy	Sensitivity	Specificity	AUC (95%CI)		Accuracy	Sensitivity	Specificity	AUC (95%CI)
MRI features	75.65%	89.13%	66.67%	0.85 (0.78–0.92)	$P_1=0.30$	76.00%	80.00%	73.33%	0.85 (0.74–0.95)
Rad-Score	76.52%	80.43%	73.91%	0.82 (0.73–0.90)	$P_2=0.13$	82.00%	60.00%	96.67%	0.80 (0.67–0.93)
Nomogram	80.87	80.43%	81.16%	0.87 (0.81–0.94)	$P_3=0.02$	82.00%	70.00%	90.00%	0.89 (0.81–0.98)

P1, AUC comparison between MRI features and Rad-score; P2, MRI features vs. Nomogram; P3, MRI Rad-score vs. Nomogram.

combining LI-RADS and radiomics features based on CEMRI demonstrated improved performance in predicting MVI, with high goodness-of-fit and clinical benefits, and this model may provide a noninvasive tool for predicting MVI and for guiding individualized treatment decision-making for HCC patients falling into the Milan criteria.

**Dear editors**

We would like to submit the enclosed manuscript entitled “A nomogram model integrating LI-RADS features and radiomics based on contrast-enhanced magnetic resonance imaging for predicting microvascular invasion in hepatocellular carcinoma falling the Milan criteria”, which we wish to be considered for publication in *Translational Oncology*. No conflict of interest exists in the submission of this manuscript, and manuscript is approved by all authors for publication. This study was performed to develop and verify a preoperative nomogram model for predicting early recurrence (ER) using clinical factors, serological markers and MRI LI-RADS v2018 features, in order to identify independent predictors about ER treated with TACE for the first time to our best knowledge, hoping to provide a personalized alternative for predicting prognosis and guiding subsequent treatment in HCC patients following TACE. We deeply appreciate your consideration of our manuscript, and we look forward to receiving comments from the

reviewers. If you have any queries, please don't hesitate to contact me.

**Declaration of Competing Interest**

The authors declare that they have no known competing financial interests or personal relationships that could have appeared to influence the work reported in this paper.

**Funding**

This work was supported by Youth Project of Changzhou Health Commission (QN202022; QN202111); Young Talent Development Plan of Changzhou Health Commission (CZQM202105).

**Author contributions statement**

All authors contributed significantly to the study conception and design, data collection, analysis and interpretation of results, draft manuscript and preparation as well as review of results and the final version of the manuscript.

## Supplementary materials

Supplementary material associated with this article can be found, in the online version, at doi:[10.1016/j.tranon.2022.101597](https://doi.org/10.1016/j.tranon.2022.101597).

## References

- [1] H. Sung, J. Ferlay, R.L. Siegel, et al., Global Cancer Statistics 2020: GLOBOCAN Estimates of Incidence and Mortality Worldwide for 36 Cancers in 185 Countries, *CA Cancer J. Clin.* 71 (3) (2021) 209–249.
- [2] A. Rizzo, M. Nannini, M. Novelli, et al., Dose reduction and discontinuation of standard-dose regorafenib associated with adverse drug events in cancer patients: a systematic review and meta-analysis, *Ther. Adv. Med. Oncol.* 12 (2020), 1758835920936932.
- [3] A. Forner, M. Reig, J. Bruix, Hepatocellular carcinoma, *Lancet Lond. Engl.* 391 (10127) (2018) 1301–1314.
- [4] G. Sapisochin, J. Bruix, Liver transplantation for hepatocellular carcinoma: outcomes and novel surgical approaches, *Nat. Rev. Gastroenterol. Hepatol.* 14 (4) (2017) 203–217.
- [5] A. Rizzo, A.D. Ricci, G. Gadaleta-Caldarola, et al., First-line immune checkpoint inhibitor-based combinations in unresectable hepatocellular carcinoma: current management and future challenges, *Expert Rev. Gastroenterol. Hepatol.* 15 (11) (2021) 1245–1251.
- [6] D.J. Erstad, K.K. Tanabe, Prognostic and Therapeutic Implications of Microvascular Invasion in Hepatocellular Carcinoma, *Ann. Surg. Oncol.* 26 (5) (2019) 1474–1493.
- [7] Y. Sugawara, T. Hibi, Surgical treatment of hepatocellular carcinoma, *Biosci. Trends* 15 (3) (2021) 138–141.
- [8] Z. Zheng, R. Guan, W. Jianxi, et al., Microvascular Invasion in Hepatocellular Carcinoma: a Review of Its Definition, Clinical Significance, and Comprehensive Management, *Wu YS, ed, J. Oncol.* 2022 (2022) 1–10.
- [9] A. Reginelli, G. Vacca, T. Segreto, et al., Can microvascular invasion in hepatocellular carcinoma be predicted by diagnostic imaging? A critical review, *Future Oncol.* 14 (28) (2018) 2985–2994.
- [10] S.B. Hong, S.H. Choi, S.Y. Kim, et al., MRI Features for Predicting Microvascular Invasion of Hepatocellular Carcinoma: a Systematic Review and Meta-Analysis, *Liver Cancer* 10 (2) (2021) 94–106.
- [11] Y.Z. He, K. He, R.Q. Huang, et al., Preoperative evaluation and prediction of clinical scores for hepatocellular carcinoma microvascular invasion: a single-center retrospective analysis, *Ann. Hepatol.* 19 (6) (2020) 654–661.
- [12] V. Chernyak, K.J. Fowler, A. Kamaya, et al., Liver Imaging Reporting and Data System (LI-RADS) Version 2018: imaging of Hepatocellular Carcinoma in At-Risk Patients, *Radiology* 289 (3) (2018) 816–830.
- [13] X. Meng, Y. Wang, J. Zhou, et al., Comparison of MRI and CT for the Prediction of Microvascular Invasion in Solitary Hepatocellular Carcinoma Based on a NON-RADIOMICS and Radiomics Method: which Imaging Modality Is Better? *J. Magn. Reson. Imaging* 54 (2) (2021) 526–536.
- [14] Q. Wang, C. Li, J. Zhang, et al., Radiomics Models for Predicting Microvascular Invasion in Hepatocellular Carcinoma: a Systematic Review and Radiomics Quality Score Assessment, *Cancers (Basel)* 13 (22) (2021) 5864.
- [15] X. Li, H. Huang, X. Yu, P. Chen, J. Ouyang, B. Huang, A novel prognostic nomogram based on microvascular invasion and hematological biomarkers to predict survival outcome for hepatocellular carcinoma patients, *Surg. Oncol.* 33 (2020) 51–57.
- [16] T.I. Huo, S.Y. Ho, C.C. Ko, Nomogram for surgical hepatocellular carcinoma: what have we missed? *Liver Int. Off. J. Int. Assoc. Study Liver* 41 (12) (2021) 3034–3035.
- [17] H. Cai, Y. Zhang, H. Zhang, et al., Prognostic role of tumor mutation burden in hepatocellular carcinoma after radical hepatectomy, *J. Surg. Oncol.* 121 (6) (2020) 1007–1014.
- [18] N. Rungsakulkij, S. Mingphruedhi, W. Suragul, et al., Platelet-to-Lymphocyte Ratio and Large Tumor Size Predict Microvascular Invasion after Resection for Hepatocellular Carcinoma, *Asian Pac. J. Cancer Prev.* 19 (12) (2018) 3435–3441.
- [19] X.Y. Lu, T. Xi, W.Y. Lau, et al., Pathobiological features of small hepatocellular carcinoma: correlation between tumor size and biological behavior, *J. Cancer Res. Clin. Oncol.* 137 (4) (2011) 567–575.
- [20] S. Usta, C. Kayaalp, Tumor Diameter for Hepatocellular Carcinoma: why Should Size Matter? *J. Gastrointest. Cancer* 51 (4) (2020) 1114–1117.
- [21] L. Song, J. Li, Y. Luo, The importance of a nonsmooth tumor margin and incomplete tumor capsule in predicting HCC microvascular invasion on preoperative imaging examination: a systematic review and meta-analysis, *Clin. Imaging* 76 (2021) 77–82.
- [22] H. Wei, H. Jiang, X. Liu, et al., Can LI-RADS imaging features at gadoteric acid-enhanced MRI predict aggressive features on pathology of single hepatocellular carcinoma? *Eur. J. Radiol.* 132 (2020), 109312.
- [23] R. Cannella, A. Furlan, Mosaic architecture of hepatocellular carcinoma, *Abdom. Radiol. N. Y.* 43 (7) (2018) 1847–1848.
- [24] J.D. Kovac, A. Ivanovic, T. Milovanovic, et al., An overview of hepatocellular carcinoma with atypical enhancement pattern: spectrum of magnetic resonance imaging findings with pathologic correlation, *Radiol. Oncol.* 55 (2) (2021) 130–143.
- [25] L. Zhang, S. Kuang, J. Chen, et al., The Role of Preoperative Dynamic Contrast-enhanced 3.0-T MR Imaging in Predicting Early Recurrence in Patients With Early-Stage Hepatocellular Carcinomas After Curative Resection, *Front Oncol.* 2020.
- [26] Z. Lei, J. Li, D. Wu, et al., Nomogram for Preoperative Estimation of Microvascular Invasion Risk in Hepatitis B Virus-Related Hepatocellular Carcinoma Within the Milan Criteria, *JAMA Surg.* 151 (4) (2016) 356–363.
- [27] H. Zhao, Y. Hua, T. Dai, et al., Development and validation of a novel predictive scoring model for microvascular invasion in patients with hepatocellular carcinoma, *Eur. J. Radiol.* 88 (2017) 32–40.
- [28] G.W. Ji, F.P. Zhu, Q. Xu, et al., Radiomic Features at Contrast-enhanced CT Predict Recurrence in Early Stage Hepatocellular Carcinoma: a Multi-Institutional Study, *Radiology* 294 (3) (2020) 568–579.
- [29] Z. Zhang, H. Jiang, J. Chen, et al., Hepatocellular carcinoma: radiomics nomogram on gadoteric acid-enhanced MR imaging for early postoperative recurrence prediction, *Cancer Imaging* 19 (1) (2019) 22.
- [30] L. Gao, M. Xiong, X. Chen, et al., Multi-Region Radiomic Analysis Based on Multi-Sequence MRI Can Preoperatively Predict Microvascular Invasion in Hepatocellular Carcinoma, *Front. Oncol.* 12 (2022), 818681.